

Article

Analysis of Rock Breaking Parameters and Simulation of Mechanical Characteristics of Multi-Nozzle Jet Impact

Yanbao Liu ¹, Lipeng He ^{2,*} , Linchao Dai ¹, Kai Shen ¹ and Quanbin Ba ¹

¹ National Key Laboratory of Gas Disaster Detecting, Preventing and Emergency Controlling, China Coal Technology Engineering Group Chongqing Research Institute, No. 55, Shangqiao No.3 Village, Shapingba District, Chongqing 400039, China; yanbao_liu@163.com (Y.L.); dailinchao@126.com (L.D.); shenkaiedu@126.com (K.S.); quanbin_ba@163.com (Q.B.)

² School of Resources and Safety Engineering, Chongqing University, Chongqing 400044, China

* Correspondence: h_lipeng@163.com

Abstract: With the continuous development of high-pressure water jet technology, research on the optimization of structural parameters for multi-nozzle configurations, the perforation effect of jet rotational impact rock breaking, and the impact force during rock breaking has received increasing attention. Through the development of a self-designed high-pressure water jet rotational drilling test device, rock breaking experiments were conducted on sandstone of different strengths using jet streams with different inclination angles, various combinations of nozzles, different target distances, and different rotational speeds. The parameters and structure of the multi-nozzle jet drill bit were optimized, and the impact of water jet-rock breaking effects was studied. The rationality of different inclination-angle jet streams in rock breaking was verified using the ALE-FEM coupling method. The changes in the force on the target body and the fragmentation mode during rock breaking with different inclination-angle jet streams were analyzed. The results showed that under the condition of adjustable inclination angles, a smaller inclination angle resulted in greater depth and a smaller diameter of rock breaking, while a larger inclination angle resulted in greater width and a smaller depth of rock breaking. The optimal combination of multi-nozzle jet streams was determined to be 20°, 30°, and 60°, which achieved a balance between rock breaking and borehole expansion performance. The efficiency of multi-nozzle jet rotational rock breaking decreased with increasing target distance, with the optimal range being 2 to 4 mm. The rotational speed of the multi-nozzle jet stream had a significant impact on rock-breaking efficiency. Under the same target distance conditions, as the drilling speed increased, the volume of rock breaking initially increased and then decreased, and the rate of volume attenuation increased with increasing target distance. The forms of rock breaking in multi-nozzle jet streams were not identical. Jet streams with smaller inclination angles mainly caused tensile failure through axial impact, while those with larger inclination angles primarily caused shear failure through radial impact. This study provides valuable guidance for optimizing the structural parameters of multi-nozzle jet drill bits and researching rotational rock breaking.

Keywords: rock breaking efficiency; structural parameters; multi-nozzle jet; rotational rock breaking; mechanical characteristics



Citation: Liu, Y.; He, L.; Dai, L.; Shen, K.; Ba, Q. Analysis of Rock Breaking Parameters and Simulation of Mechanical Characteristics of Multi-Nozzle Jet Impact. *Sustainability* **2023**, *15*, 12414. <https://doi.org/10.3390/su151612414>

Academic Editor: Jianjun Ma

Received: 24 June 2023

Revised: 9 August 2023

Accepted: 11 August 2023

Published: 15 August 2023



Copyright: © 2023 by the authors. Licensee MDPI, Basel, Switzerland. This article is an open access article distributed under the terms and conditions of the Creative Commons Attribution (CC BY) license (<https://creativecommons.org/licenses/by/4.0/>).

1. Introduction

High-pressure water jet technology is one of the main production enhancement technologies for deep coal bed methane exploitation, unconventional natural gas exploitation, and oil drilling [1]. These technologies mainly include hydraulic punching [2], hydraulic slotting [3], hydraulic fracturing [4], and radial drilling [5]. In recent years, with the gradual increase in the depth of energy extraction, such as coalbed methane and oil and gas reservoirs, the reservoir environment with high in situ stress and low permeability has become more and more obvious [6]. Hydraulic punching and hydraulic fracturing have limited impact on coal seam permeability, while hydraulic fracturing involves high fracture

pressure and increased risk, with very limited effects on reservoir modification. In recent years, some scholars have proposed the use of high-pressure water jet drill bits to construct multiple branch holes through a guide device in the target layer, thereby increasing gas flow channels, improving coal mine gas drainage efficiency, and reducing gas disasters. This technology has attracted widespread attention from domestic and international scholars due to its advantages in rock breaking and deep drilling capabilities [7–9]. Among them, the rock-breaking mechanism and the influence of rotational speed on rock breaking by multi-nozzle jet drill bits have become the main research hotspots for this technology. However, existing research lacks optimization of parameters for multiphase jet streams and the study of rock-breaking mechanisms caused by jet impacts.

Currently, both domestic and foreign scholars have conducted numerous experiments on the theory and efficiency of water jet rock breaking. Cao et al. [10] conducted fragmentation tests on coal, sandstone, and raw coal using jet impacts. They analyzed the fracture mechanism under different jet pressures and quantitatively analyzed the size of the damaged area. Lu et al. [11] used high-speed jet impacts on sandstone to study the failure modes and crack propagation patterns under high-speed water jet impacts. They observed and analyzed the crack extension in sandstone to better understand its failure mechanism. They also quantified the entire process of jet impact on sandstone and the distribution of dynamic pressure using the finite element method, and they studied the fragmentation pattern of water jet impacts on laterally isotropic rocks. Li et al. [12] conducted tests on the impact of multi-nozzle jet streams on target distance and impact pressure, analyzing the rock breaking and perforation effects under different operating conditions. Li et al. [13] analyzed the threshold pressure for multi-nozzle jet rock breaking and suggested that the rules of multi-nozzle jet drilling can be better applied in petroleum drilling. Reinsch et al. [14] analyzed the jet impact cloud by high-speed camera and studied the dynamic phenomenon of jet impact. Ma et al. [15] conducted a study that combined experiments and models to investigate the impact of shockwave propagation and energy absorption on material damage.

The rock breaking efficiency of high-pressure water jets is influenced by various factors such as nozzle structure, flow field characteristics, jet pressure, and the physical properties of coal and rock, which makes the process of jet rock breaking extremely complex [16–19]. With the development of numerical simulation technology, material crushing and its change process analysis can be better reflected [20]. Numerical simulation methods have provided possibilities for studying the dynamic fragmentation process of rocks and analyzing the changes in their stress during water jet impact [21]. Understanding the impact load and dynamic response characteristics of rocks during high-pressure water jet rock drilling is an important aspect of studying the mechanism of high-pressure water jet rock breaking [22]. To this end, Jiang et al. [23] used the SPH/FEA method to analyze the formation state of jet-fractured rocks and the propagation of rock fractures. Liu et al. [24] simplified continuous jets into smooth particles at different angles using the SPH method to analyze the impact of different jet angles on coal and rock. They obtained variations in rock energy, erosion depth, and width during the fragmentation process. Xue et al. [25,26] employed the Arbitrary Lagrangian–Eulerian Finite Element Method (ALE-FEM) to study the fracturing mechanism of single-nozzle jet impact on coal. They reconstructed the damaged area of jet-impacted coal and obtained the shapes of the perforations at different times. Ni et al. [27] simulated the process of water jet rock breaking using a nonlinear dynamic finite element method. The results showed that the rock fragmentation process first formed a circular fracture zone, which then developed radially and axially, resulting in a conical-shaped crack pit. Ma et al. [28] implemented the Johnson–Holmquist–Beissel (JHB) model within a four-dimensional lattice spring framework, enabling the consideration of material nonlinearity, dynamic variations, and fracture behavior in simulations. They then applied this implementation to the issue of projectiles penetrating materials to study the interactions between projectiles and different materials. The outcomes of this study

hold significant importance for comprehending material response behaviors in high-speed collisions and penetration scenarios.

In conclusion, although many scholars have conducted research on the process of jet impact rock breaking and the forms of rock fragmentation based on single-nozzle jets, there are few reports on the analysis of nozzle angle selection and jet impact forces, especially for multi-nozzle jet rotational rock breaking. Additionally, multi-nozzle jets are significantly influenced by jet impact distance, rotational speed, and rock properties during rotational rock breaking. Therefore, the authors conducted experiments using a self-designed test platform to analyze the impact of rock breaking efficiency under different rock target distances, rotational speeds, and rock strengths. The ALE-FEM coupling algorithm will be used to construct a multi-nozzle jet impact rock breaking model to obtain the rock breaking effects of different nozzle angles and analyze the stress state and rotation of the rock breaking process of multi-nozzle jet impact rock breaking. The aim of this study is to optimize the multi-nozzle jet drilling head to improve rock breaking efficiency and provide technical support for the application of radial drilling technology. This study can lay a theoretical foundation for the sustainable development of coal mine safety production and can form a sustainable key technology for future coal mine gas disaster management.

2. Drill Bit Model and Experimental System

2.1. Multi-Nozzle Jet Drilling Bit Model

The main factors influencing the efficiency of high-pressure water jet rock breaking include the structural parameters of the drilling head, hydraulic parameters, and mechanical parameters of the rock formation. Among them, the nozzle parameters of the rock drilling head have the most significant impact on rock breaking. The multi-nozzle water jet drilling head mainly consists of three components: the rotating body, the drill head casing, and the connecting end, with the rotating body being the core component for rock breaking. The key structural parameters of the front-end rotating body include the nozzle diameter, nozzle inclination angle, and number of nozzles. Figure 1 shows the structure of the rock-breaking nozzle's rotating body. High-pressure water enters from the inlet at the rear of the rotating body and is conveyed through the internal channel to the front-end rock-breaking nozzles. The rock-breaking nozzles are designed with different inclined angles asymmetrically, and as they rotate, they complement each other to break the rock, reduce the blind spot of fragmentation, and improve the efficiency of rock breaking. Among them, the first nozzle and the second nozzle are the main rock-breaking nozzles, and the third nozzle is the auxiliary rock-breaking nozzle. Nozzles less than 45° are defined as primary rock-breaking nozzles, and nozzles larger than 45° are auxiliary rock-breaking nozzles. θ represents the angle between the nozzle and the central axis of the drill head, and S represents the distance from the nozzle outlet to the center of the drill head. Since the nozzle diameter has a significant impact on the hydraulic impact force of the water jet, it is necessary to calculate and analyze the nozzle diameter in this study.

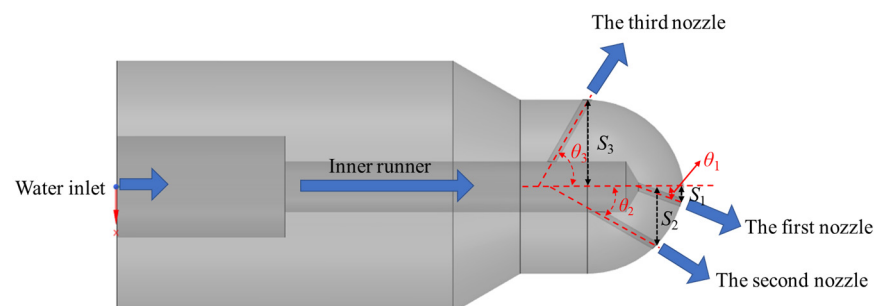


Figure 1. Rotating body structure.

The nozzle diameter can be obtained according to the actual flow rate; assuming Q is an ideal fluid, we can derive the following equation:

$$Q = \frac{1}{4}\pi d^2 \rho \sqrt{\frac{2P}{\rho}}, \quad (1)$$

where Q is the jet flow; d is the nozzle diameter; P is the jet pressure; and ρ is the fluid density.

For a single nozzle, the relationship between the nozzle diameter, jet pressure, and flow rate is obtained from the below formula as follows:

$$d = \sqrt{\frac{4q}{\pi \rho \sqrt{\frac{2P}{\rho}}}}. \quad (2)$$

The diameter of the nozzles in a multi-nozzle jet drilling tool can be calculated based on the relationship between the equivalent nozzle diameter and the individual nozzle diameter as follows:

$$D = \sqrt{d_1^2 + d_2^2 + \dots + d_n^2}, \quad (3)$$

in the equation, d_n represents the diameter of the n th nozzle.

The selection of individual nozzle diameters is determined based on the inner diameter of the high-pressure hose. The inner diameter of the high-pressure hose used in this article is 4 mm, so it can be determined that the diameter of 1.0 mm meets the experimental conditions.

2.2. Experimental System

The experiment utilizes a self-designed and developed high-pressure water jet rotary drilling test system. The system mainly consists of three major components: the power supply system, the control system, and the rock-breaking drilling system. As shown in Figure 2, the power supply system includes a 1 m³ water tank and a high-pressure water pump with a maximum working pressure of 100 MPa and a rated flow rate of 100 L/min. The control system includes a pneumatic pressure-regulating valve, a foot valve, and a rotary control device. The pneumatic pressure regulating valve is connected to the high-pressure water pump, and the foot valve is installed in the middle of the high-pressure hose to ensure safety pressure relief. The rotary control device can adjust the rock-breaking target distance, rotational speed, and drilling speed. The rock-breaking drilling system consists of a test platform, a stepper motor, a servo motor, a high-pressure rotary joint, and a specimen fixture. The stepper motor has a maximum torque of 20 N/m, the servo motor has a maximum speed of 2800 rpm, the high-pressure rotary joint has a maximum speed of 2000 rpm, and the maximum load pressure is 150 MPa. The rock-breaking nozzle is installed at the front end of the rotary component and can be precisely controlled for the rock-breaking target distance and rotational speed through the control device.

2.3. Experimental Materials and Procedures

Experimental research on the characteristics that influence multi-factor rock fracturing and perforation requires extensive experimental work. In order to facilitate the rapid installation and disassembly of rock specimens during the experiment, a clamping-type quick-release specimen fixture has been designed in this study. It is capable of clamping cylindrical specimens with a diameter of $\Phi 100$ mm. Sandstone is selected as the main specimen for the multi-parameter experiments due to its excellent homogeneity, which allows for better observation and understanding of the experimental phenomena and patterns after rock fracturing and perforation. As shown in Table 1, the basic physical and mechanical parameters of the three sandstone types used in this chapter are presented. Some rock specimens are illustrated in Figure 3.

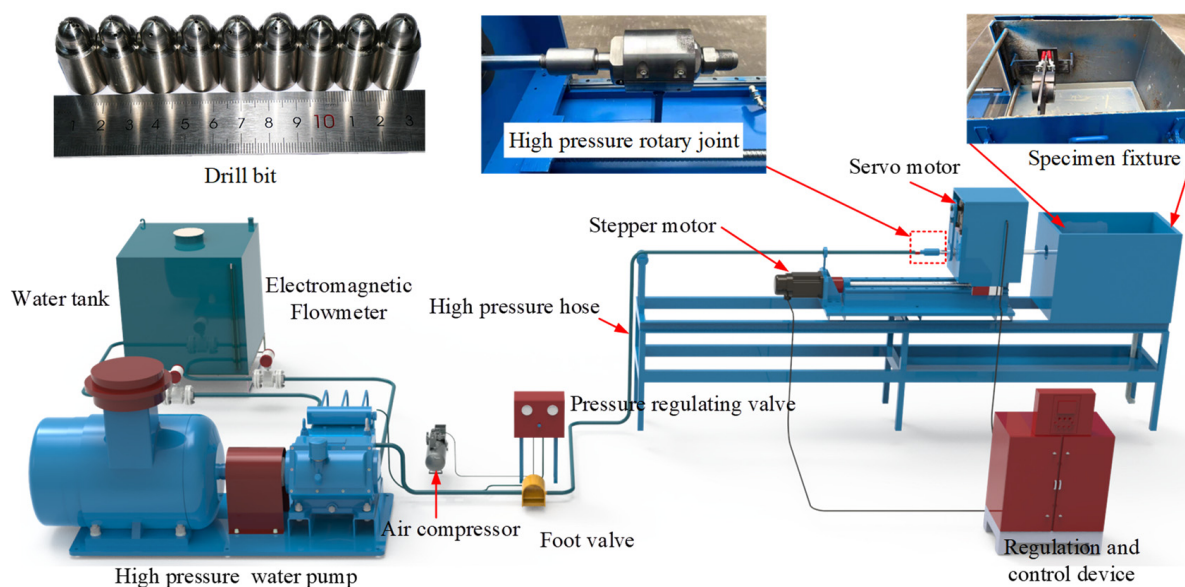


Figure 2. High-pressure water jet rotary drilling experimental device.

Table 1. Physical and mechanical properties of the sandstone samples.

Parameters	Density (g/cm ³)	Tensile Strength (MPa)	Uniaxial Compressive Strength (MPa)	Elastic Modulus (GPa)
Coarse sandstone	2.14	4.48	38.8	33
Fine sandstone	2.27	8.26	58.9	35.5
Bluestone	2.42	12.49	97	40.2



Figure 3. Rock specimens.

This study primarily employed the method of controlling variables to investigate the impact of jet angles, different combinations of jet angles, target distance, rotational speed, and rotational speed on rocks of different strengths. The parameters are listed in Table 2. The nozzle diameter was set at $d = 1.0$ mm, and the single-nozzle jet pressure was set at 20 MPa, while the multi-nozzle jet pressure was set at 40 MPa.

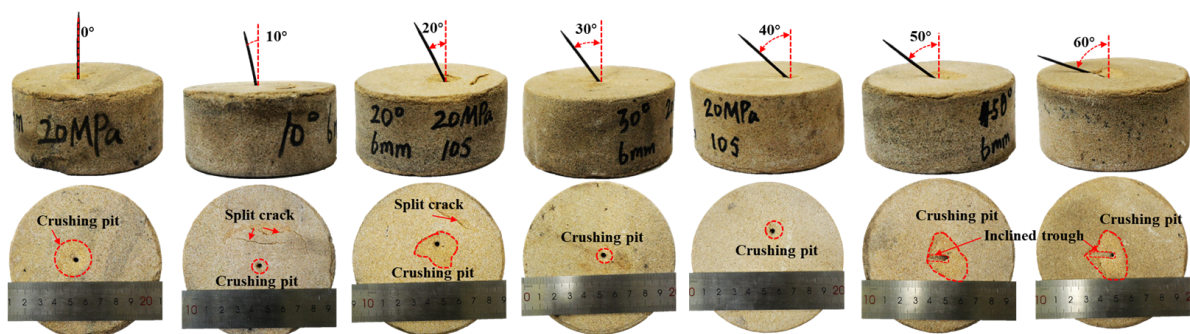
Table 2. Experimental parameters.

Types	Parameters
Jet angle	0°, 10°, 20°, 30°, 40°, 50°, 60°
Jet pressure	20 MPa, 40 MPa
Rotational speed	100 rpm, 200 rpm, 400 rpm, 600 rpm, 800 rpm, 1000 rpm
Rock-breaking standoff distance	2 mm, 4 mm, 6 mm, 8 mm, 10 mm

3. Results and Discussion

3.1. Influence of the Jet Angle on Rock Breaking

To investigate the influence of jet angles on rock impact and fragmentation performance, experiments were conducted using a single-nozzle jet at different angles. The jet pressure was set at 20 MPa, the standoff distance was 6 mm, and the erosion time was 10 s. Rock fragmentation tests were carried out at jet angles of 0°, 10°, 20°, 30°, 40°, 50°, and 60°, and the impact and fragmentation effects were analyzed, as shown in Figure 4. By observing the rock fragmentation effects at different jet angles in Figure 4, it can be observed that as the angle increases, the inclined grooves formed by the jet impact become larger and the fragmentation craters become more pronounced. At a jet angle of 0°, the jet vertically impacts the rock surface, resulting in regular fracture cavities. At 10° and 20°, noticeable cracks form on the rock surface due to jet impact, but no rock detachment occurs. The fragmentation crater formed by the 20° jet angle is significantly larger than that formed by the 10° angle. At 30° and 40°, although no obvious fracture cracks form, the shape of the fragmentation craters indicates significant expansion in the direction of the jet inclination. Observing the fragmentation craters formed by the 50° and 60° jet angles, it can be seen that they are the largest. This is mainly due to the high radial impact energy generated by the jet, which leads to the formation of splitting cracks inside the rock. As the jet continues to impact with significant energy, the cracks further expand, resulting in the collapse of the upper rock blocks and the formation of larger fragmentation craters. It is well known that the axial velocity of the jet decreases as the jet angle increases, while the radial velocity increases with the jet angle. However, due to the extremely short duration of the high-pressure water jet rock fragmentation process, experimental methods alone are insufficient to fully reveal the rock fragmentation mechanism. Therefore, subsequent analysis will be conducted through numerical simulations to further examine the stress state of rock under the impact of jets at different angles.

**Figure 4.** Rock-breaking effect of jets with different angles.

3.2. Different Combinations of Multiple-Nozzle Rock-Breaking Effects

In order to further analyze the rock-breaking effect of different combinations of angled jets and obtain the optimal parameters for the multi-nozzle jet drilling tool, rock-breaking experiments were conducted using different combinations of angled nozzles. The experimental parameters for the multi-nozzle drilling tool are shown in Table 3. To visually analyze the shape of the fragmentation cavity and the volume of rock breaking. The jet

pressure was set at 40 MPa, the jet standoff distance was 2 mm, the rotational speed was 200 rpm, and the erosion time was 20 s.

Table 3. Parameters of the multi-nozzle bit.

Serial Number	Jet Inclination/ $^{\circ}$ (θ_1 - θ_2 - θ_3)	Eccentric Distance of Nozzle (mm)		
		S ₁	S ₂	S ₃
1#	10-25-45	0.5	3	4
2#	10-30-45	0.5	3.5	4
3#	20-30-40	1	3.5	3.8
4#	10-30-50	0.5	3.5	4.2
5#	15-25-50	0.75	3	4.2
6#	20-30-50	1	3.5	4.2
7#	10-30-60	0.5	3.5	4.5
8#	15-30-60	0.75	3.5	4.5
9#	15-35-60	0.75	3.75	4.5
10#	20-30-60	1	3.5	4.5

Figure 5 shows the morphology of rock fragmentation for different combinations of angled jets in the multi-nozzle configuration. The multi-nozzle jet flow primarily forms a main fragmentation zone and an auxiliary fragmentation zone, where the main fragmentation zone is formed by the first nozzle and the second nozzle and the auxiliary fragmentation zone is formed by the third nozzle. To quantify the changes in the fragmentation cavity, measurements of fragmentation diameter and fragmentation volume were conducted, and the results are shown in Figure 6. As the angle of the third nozzle increases, the diameter of the fragmentation cavity becomes larger. However, it can be clearly observed from Figure 5 that as the diameter increases, the depth of fragmentation decreases. When the angle of nozzle 1 is smaller, the depth of impact fragmentation increases, and the borehole diameter becomes smaller. Similarly, the rock-breaking patterns of the second nozzle are similar to those of the first nozzle. However, the spacing between the first nozzle and the second nozzle and the difference in nozzle angles have a significant impact on the rock-breaking efficiency. For example, in the case of rock #6, the difference in angle between the first nozzle and the second nozzle is 20° , resulting in an excessively large protruding cone and a very small diameter of the fragmentation hole. The volume of rock fragmentation initially decreases, then increases, and eventually stabilizes as the nozzle angle increases. For nozzles with smaller angles, the depth of rock fragmentation is greater. Although the aperture size decreases, the rotating conditions weaken the formation of the central protrusion. On the other hand, larger angles are not conducive to borehole formation. By comparing the fractured boreholes of #8, #9, and #10, it was found that the volume of rock fragmentation and the variation in borehole diameter were relatively small, resulting in regular borehole formation, which is conducive to continuous drilling. Based on the quantitative analysis of this experimental study and subsequent parameter research, the combination of angled jets with angles of 20° , 30° , and 60° was selected as the optimal parameter combination for the multi-nozzle jet drilling tool.

3.3. The Impact of Standoff Distance on Rock Fragmentation

Figure 7 illustrates the rock fragmentation and drilling effects of a multi-nozzle jet under the conditions of 40 MPa pressure, 100 rpm rotational speed, and 20 s erosion time at different rock standoff distances. The experiments indicate that as the standoff distance increases, the diameter of the auxiliary fragmentation zone formed by rock fragmentation becomes larger. The blind zone of fragmentation also increases with an increase in standoff distance, while the diameter of the main fragmentation zone begins to increase when the standoff distance reaches a certain value. The auxiliary fragmentation zone, formed by a 60° jet, creates a fragmentation ring. At a standoff distance of 2 mm, the diameter of the fragmentation ring is 4.9 cm, and it increases to 7.5 cm when the standoff distance

reaches 10 mm. The diameter of the blind zone increases from 0.6 cm to 1.4 cm. The main fragmentation zone, at standoff distances of 2 mm to 6 mm, forms craters with a diameter of 2.1 cm. However, when the standoff distance reaches 8 mm, the diameter of the main fragmentation zone becomes 2.4 cm. From the shape of the craters, it can be observed that as the standoff distance increases, the depth of the main fragmentation zone decreases significantly, and the protrusion becomes larger. The depth of the auxiliary fragmentation zone also decreases. Prior research has shown that the impact pressure of the jet gradually decreases with an increase in standoff distance [29,30]. Additionally, as the jet travels a longer distance, it tends to entrain more air, resulting in greater energy loss. Therefore, a larger standoff distance leads to weaker rock fragmentation capabilities. However, within the range of 2 mm to 6 mm standoff distances, the diameter of the main fragmentation zone remains relatively unchanged. This is mainly because the energy of the jet does not experience a sharp decline with an increase in standoff distance within a certain range. When the jet impacts the rock surface and forms a crater, the rebounding jet causes secondary expansion of the borehole, resulting in an increase in the diameter of the main fragmentation zone.

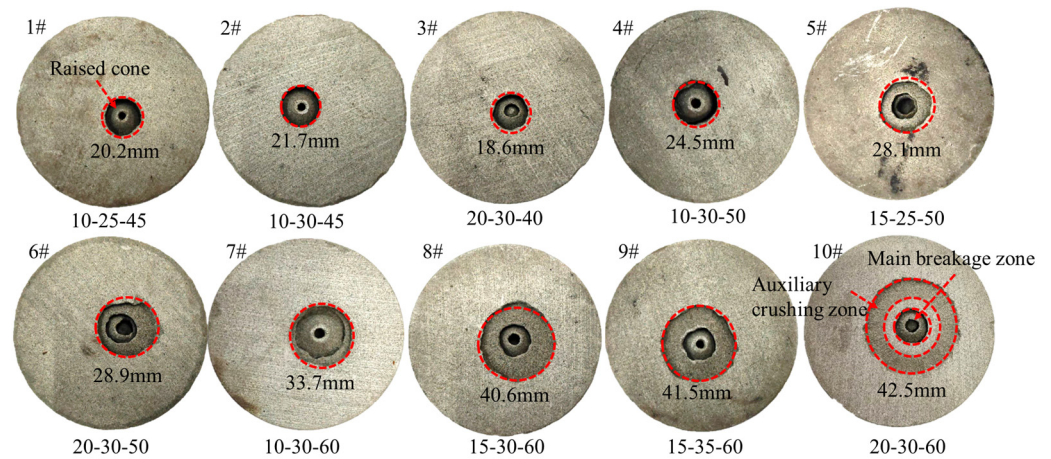


Figure 5. Rock-breaking shapes of different combinations of multi-nozzles.

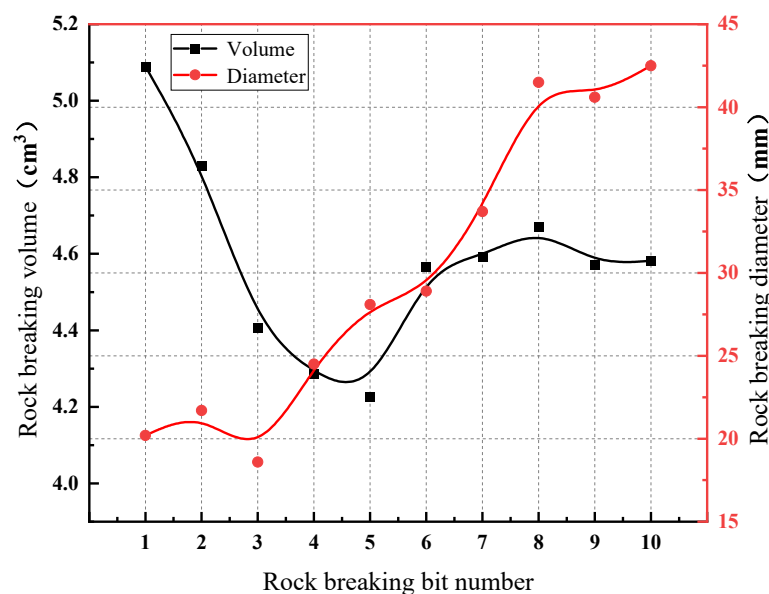


Figure 6. Rock-breaking law of bits with different parameters.

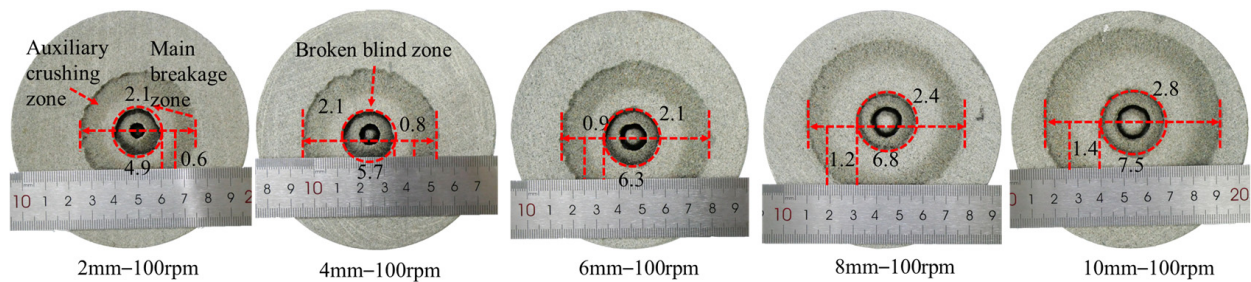


Figure 7. Rock-breaking effect with different standoff distances.

3.4. The Influence of Different Rotational Speeds on Rock Fragmentation Effects

One of the main influences on the rotary rock fragmentation of multi-nozzle jets is the rotational speed of the drill bit. Figure 8 illustrates the impact of different rotational speeds on the rock fragmentation volume of bluestone using multi-nozzle jets. The rock fragmentation conditions include a jet pressure of 40 MPa and an erosion time of 20 s. From the changing trend of the curves in the graph, it can be observed that the rock fragmentation volume decreases with increasing target distance. Under the same target distance conditions, the rock fragmentation volume initially increases and then decreases as the rotational speed increases. Moreover, the rate of decrease in rock fragmentation volume increases with increasing target distance. It can be seen from the curves in the graph that when the rotational speed increases from 800 rpm to 1000 rpm, the rate of decrease in rock fragmentation volume significantly increases. When the target distance is 2 mm and the rotational speed is 200 rpm, the maximum rock fragmentation volume is 4.08 cm^3 . However, when the rotational speed reaches 1000 rpm, the rock fragmentation volume decreases to 2.67 cm^3 . Additionally, the rock fragmentation volume at rotational speeds between 200 rpm and 400 rpm is significantly larger than at other rotational speed conditions. At a target distance of 2 mm, the rate of decrease in rock fragmentation volume is 34.6%, which increases to 63.5% when the target distance increases to 10 mm.

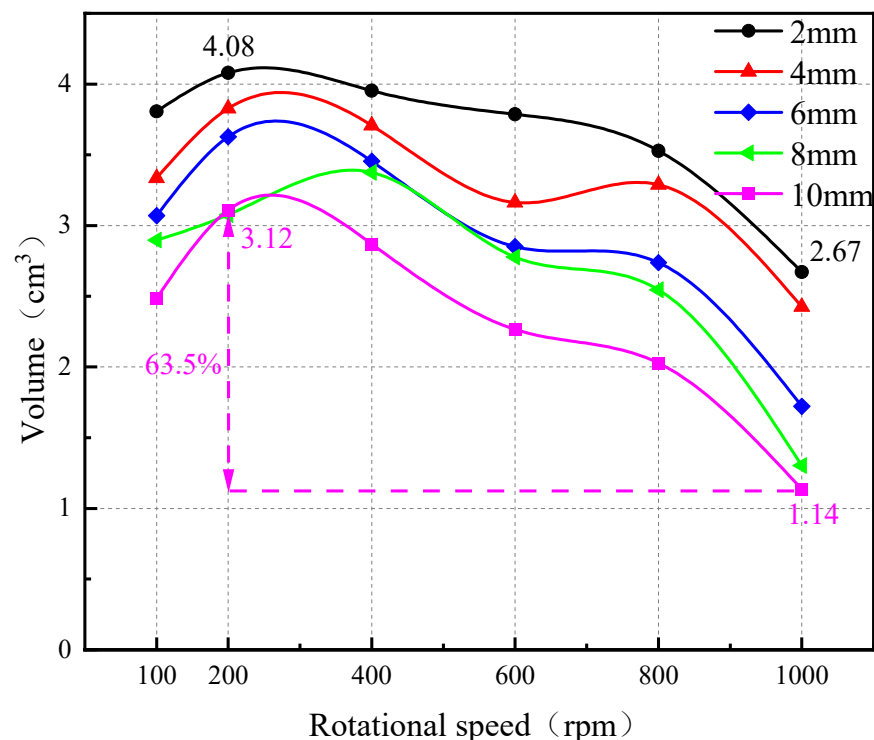


Figure 8. The influence of rotational speed on the volume of broken rock.

Based on the experimental observations, it can be concluded that there is a critical value for the rotational speed of multi-nozzle jets under the same target distance conditions. When the rotational speed is below the critical value, the impact frequency of the jets on the rocks decreases within the same rock fragmentation time, resulting in a lower total energy of jet impact on the rocks and a reduction in rock fragmentation volume. Conversely, when the rotational speed exceeds the critical value, the impact frequency of the multi-nozzle jets on rock fragmentation increases compared to lower rotational speeds. However, due to the increased rotational speed, the impact time of the jet at a specific point becomes shorter, and the jet rotates to the next fracture point before the impact kinetic energy of the jet is fully released. As a result, the accumulated energy within the rocks is insufficient to meet the destruction requirements, leading to a decrease in rock fragmentation efficiency. Furthermore, when the multi-nozzle jets rotate at high speeds, the jet structure deviates due to the increased rotational speed. The higher the rotational speed, the more severe the jet deviation, resulting in increased jet divergence and a decrease in the effective impact kinetic energy of the jet, thus reducing rock fragmentation efficiency.

3.5. The Impact of Rotational Speed on the Fragmentation of Rocks with Different Strengths

According to the findings in Section 3.4, it was discovered that rotational speed has a significant impact on rock fragmentation efficiency. To investigate whether this impact pattern applies to rocks with different strengths, experiments were conducted in this section to compare the rotational fragmentation effects on three different-strength sandstones. Figure 9 shows a comparison of the fragmentation effects on sandstones of three different strengths under the conditions of a 4 mm target distance, 20 s erosion time, a rotational speed of 100 rpm, and a jet pressure of 40 MPa. Upon observation, it was noted that under the same fragmentation conditions, the diameter of the main fragmentation zone was consistent at 2.1 cm for all three sandstones. However, the diameter of the auxiliary fragmentation zone decreased as the strength of the rock increased. The main fragmentation zone of the coarse sandstone exhibited no protrusion, while the fine sandstone had a small protrusion, and the bluestone showed a distinct protrusion in the main fragmentation zone.

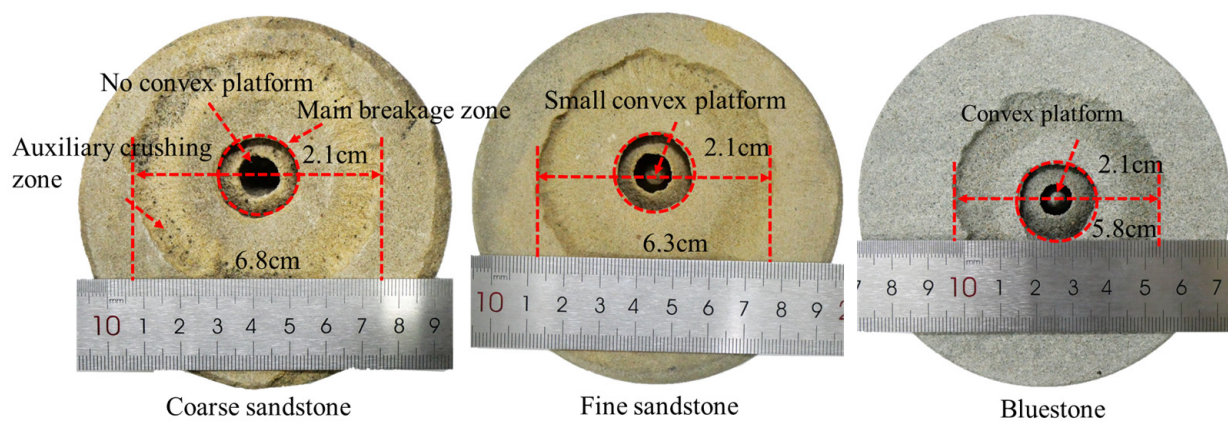


Figure 9. Comparison of the crushing of rocks with different strengths.

As shown in Figure 10, a comparison of the volume of different-strength sandstones under the impact of different rotational speeds is presented. It can be observed that the fragmentation volume of the coarse sandstone and fine sandstone increases with the increase in rotational speed. However, the fragmentation volume of the bluestone initially increases and then decreases as the rotational speed increases. Furthermore, the coarse sandstone exhibits a significant increase, reaching a maximum fragmentation volume of 29.66 cm³. Combining Figures 9 and 10, it can be concluded that the size of the auxiliary fragmentation zone is directly related to the compressive strength of the rock. Lower rock strength corresponds to a smaller threshold for jet fragmentation. When the jet impacts

the rock surface, it generates axial and radial impact forces, which determine the width of the fragmentation pit. As the multi-nozzle jet starts to rotate, different rotational speeds cause slight deflection of the jet, resulting in varying degrees of attenuation in the impact kinetic energy. However, the remaining kinetic energy after attenuation is still capable of fragmenting rocks with lower strength. In the case of low-strength rocks, the main fragmentation zone does not form a protrusion, indicating that the radial impact of the jet contributes to the destruction of the central protrusion in low-strength rocks. Therefore, the fragmentation volume of low-strength rocks increases with increasing rotational speed.

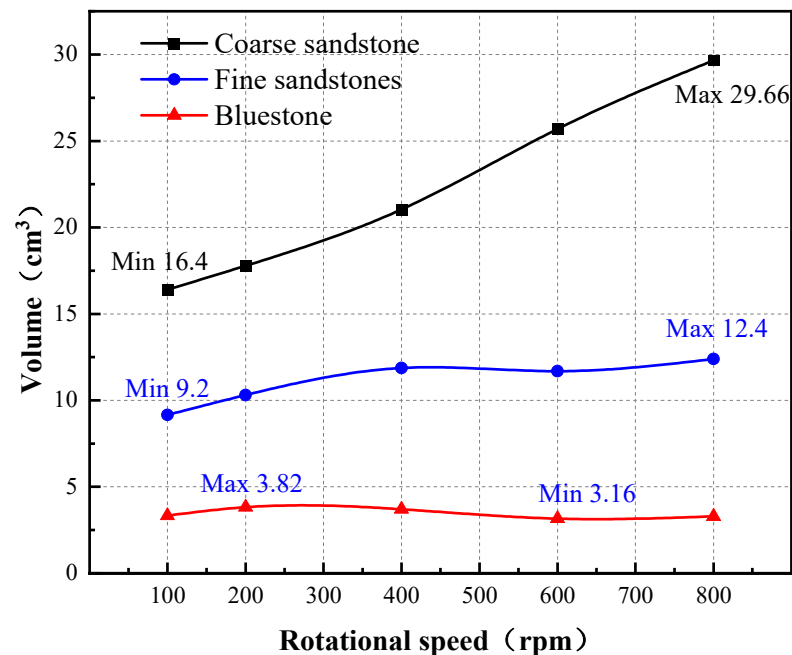


Figure 10. Influence of rotating speed on crushing volume of rock with different strengths.

Similarly, for hard rocks, greater radial impact kinetic energy is required to break the central protrusion. Therefore, when fragmenting low-strength rocks without atomization of the jet, increasing the rotational speed appropriately can achieve a larger rock fragmentation efficiency. Conversely, when fragmenting hard rocks, it is necessary to reduce the rotational speed appropriately to achieve better fragmentation results.

4. The Analysis of the Forces Acting on Rock during Continuous Jet Impact

During the process of a high-pressure water jet impacting rock, the force state of the water jet impacting the rock determines the main form of rock fragmentation. However, due to the high pressure and fast impact velocity characteristics of the jet during the rock-breaking process, the time of rock fragmentation is extremely short, especially in the case of multi-nozzle continuous jet impact, which makes the process highly complex. In the process of multi-nozzle jet impact on rock, the effect of jet impact at different angles and the subsequent changes in the stress of rock microelements during the rock-breaking process vary. Therefore, it is necessary to conduct an in-depth analysis of the mechanical relationship between multi-nozzle jet impacts. However, currently, there is limited analysis of the forces exerted by jets on rocks during water jet rock-breaking processes, and experimental methods are challenging to observe the mechanical changes during rock fragmentation. Through exploration and research by scholars, it has been found that the LS-DYNA simulation software can be used for impact dynamics analysis [31]. Therefore, based on the ALE-FEM (Arbitrary Lagrangian–Eulerian Finite Element Method) coupling method, this paper simulates and analyzes the process of multi-nozzle jet impact on rock to investigate the mechanical changes that occur during rock fragmentation.

4.1. Model Simplification and Assumptions

In order to study the stress effects of water jet impact on rocks, it is necessary to simplify the geometric model of water jet rock fragmentation, as shown in Figure 11. The process of jet fragmentation involves the interaction between high-pressure water and rocks as it flows out of the nozzle. Therefore, before numerical simulation, it is necessary to determine the relationship between pump pressure and the impact velocity of the nozzle diameter. In practical modeling, the jet fragmentation is simplified as the interaction between a high-pressure water column with a certain velocity and the rock, as shown in Figure 12. The size of the rock is $\Phi 60 \text{ mm} \times 20 \text{ mm}$. The jet nozzle is simplified as a thin-shell rotating body, and the water jet is simplified as a cylindrical body with a certain impact velocity. The jet does not come into direct contact with the rock wall. An air domain is set at the contact location between the jet and the rock. The main contact type is the meshed finite element contact type.

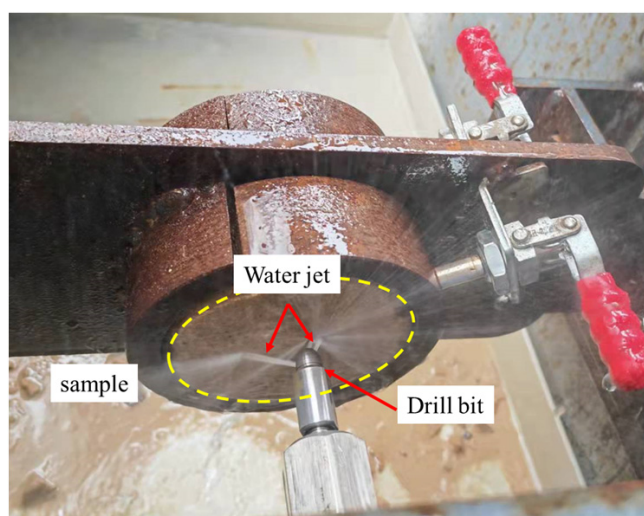


Figure 11. A water jet impacts a rock.

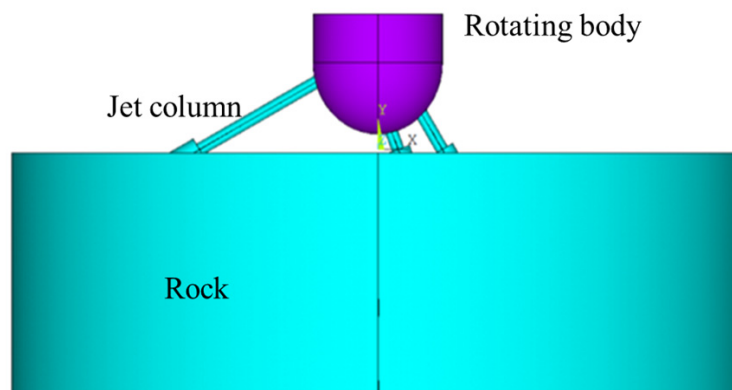


Figure 12. Simplified model of jet impact on rock.

There are multiple factors affecting the process of multi-nozzle continuous jet impact rock fragmentation. In order to facilitate calculations, the following model assumptions are proposed:

- (1) Neglecting the jet divergence phenomenon during the jet ejection process;
- (2) Neglecting the deflection effect of the jet during the rotational process;
- (3) The rock model is assumed to be isotropic.

4.2. Model Parameters and Mesh

This study employs the ALE-FEM (Arbitrary Lagrangian–Eulerian Finite Element Method) coupling algorithm for dynamic simulation of rock fragmentation under continuous water jet impact from multiple nozzles. The water jet is modeled using the NULL material model to avoid the influence of stress and strain generated by the jet during the computation. The rock model adopts the Johnson–Holmquist–Beissel (HJC) constitutive model, which has been extensively studied and proven to be suitable for high-stress and large deformation problems in rock materials. The simulation of multi-nozzle jet impacts is conducted using established governing equations, such as the state equation and yield strength function [32,33]. The numerical simulation material parameters are shown in Table 4. The parameters of water are shown in Table 5.

Table 4. HJC constitutive model parameters.

ρ (g/cm ³)	G (GPa)	f_c (GPa)	A	B	N	C	S_{Fmax}	D ₁	D ₂
2.14	13.1	0.0388	0.78	1.6	0.61	0.007	7.0	0.04	1
T (GPa)	E_{Fmin} (GPa)	K_1 (GPa)	K_2 (GPa)	K_3 (GPa)	μ_{lock}	P_{lock} (GPa)	μ_{crush}	P_{crush} (GPa)	E (GPa)
0.00448	0.01	85	−171.5	208.5	0.38	0.25	0.0013	0.017	33

Table 5. Parameters of water.

Parameter	C (m/s)	S1	S2	S3	γ_0	a	E
Water	1050	2.56	−1.986	0.2268	0.4934	0.47	2.895×10^{-6}

To ensure that the rock does not experience relative movement during the water jet impact, non-reflective boundary constraints are applied to the rock boundaries. The velocity inlet boundary condition is applied to the jet, and the velocity is decomposed in the X, Y, and Z directions using trigonometric functions to facilitate the calculation of the rotational process. The rotational body is defined as rotating around the Y-axis. After determining the geometric model, the finite element method is used for numerical discretization of the model, as shown in Figure 13. The ALE mesh is used for the air and water domains. Since jet divergence is not considered, the jet nozzle is modeled as a cylindrical body with dimensions of $\Phi 1 \text{ mm} \times 1 \text{ mm}$. The main body of the air model is a cylindrical body with dimensions of $\Phi 4 \text{ mm} \times 15 \text{ mm}$. The rock model is a cylindrical body with dimensions of $\Phi 60 \text{ mm} \times 20 \text{ mm}$, composed of Lagrange elements. The rotational body model consists of a cylindrical shell with dimensions of $\Phi 10 \text{ mm} \times 4 \text{ mm}$ and a hemispherical shell with a diameter of $\Phi 10 \text{ mm}$.

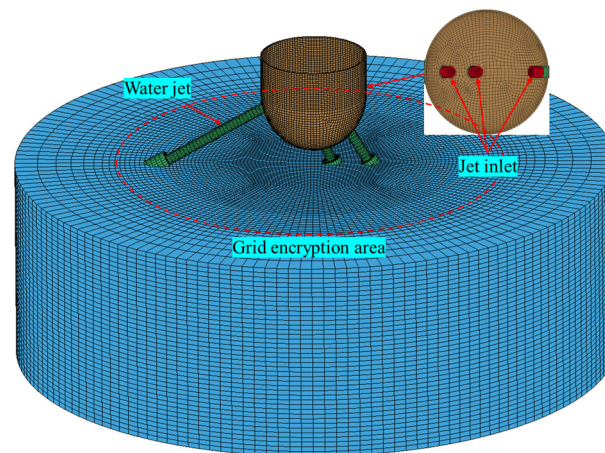


Figure 13. Grid of the rock-breaking model.

4.3. Numerical Simulation Results Analysis

4.3.1. Effect of Jet Inclination Angle

The impact force generated by the high-pressure water spraying process can be decomposed into two directions: parallel surface and vertical surface, and the depth and width of the crushing pit are expressed by the impact of these two parts. In this paper, a numerical model of different inclination jets on rocks is established, and the influence of different inclination jets on rock fragmentation effects is studied. The jet inclination angles are 0° , 10° , 20° , 30° , 40° , 50° , 60° , and 65° , respectively. The jet has a diameter of 1.0 mm, a velocity of 250 m/s, and an erosion time of 250 μs . Figure 14 shows the shape of the crushing pit formed by the rock breaking of the jet at different inclination angles. With the increase in the inclination angle of the jet, the vertical depth of the crushing pit gradually decreases while the axial width gradually increases.

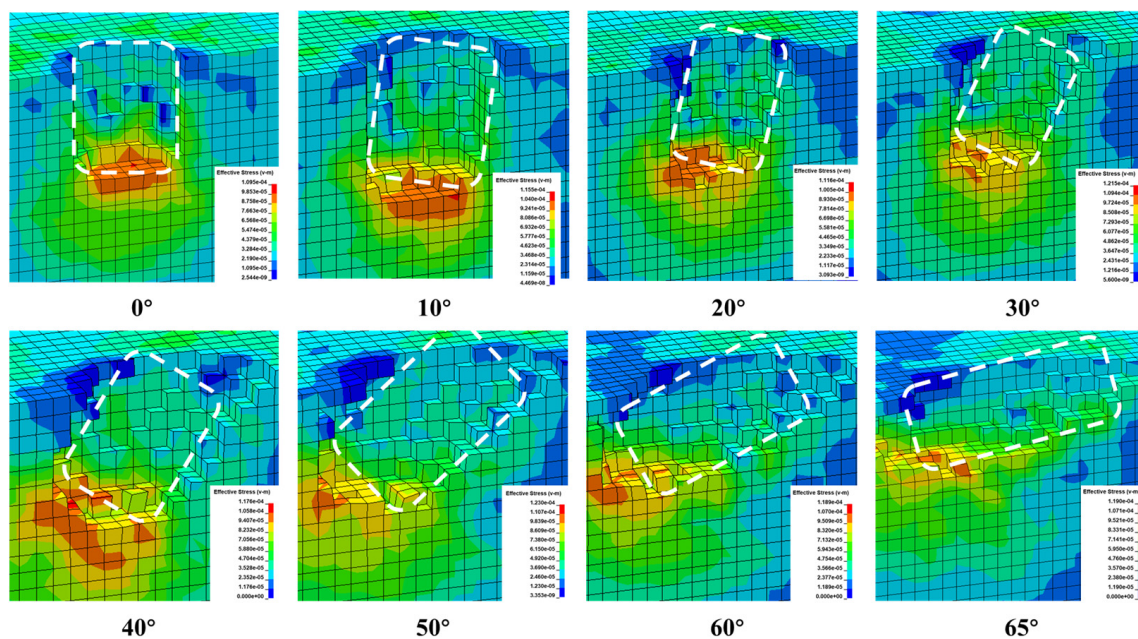


Figure 14. Different inclination angles for jet-breaking pit shapes.

Different inclination angles of the water jet have varying effects on rock fragmentation and perforation, as shown in Figure 15, which presents the numerical simulation results for different jet inclination angles. From the graph, it can be observed that as the jet inclination angle increases, the width of rock fragmentation significantly increases, while the depth of fragmentation gradually decreases. However, the volume of fragmented rock shows a trend of initially increasing, then decreasing, and finally increasing again. Since the experiment is in seconds and the numerical simulation is in milliseconds, the numerical simulation results in the figure are quite different from the experimental results, but because the change trend is basically the same, the rationality of the simulation results can be considered.

When the inclination angle is 0° , the water jet causes the greatest depth of fragmentation, with the smallest width and volume, and the depth exceeding the width. For a 10° inclination angle, the depth and width of fragmentation are roughly equal. However, as the inclination angle increases from 20° , the depth of fragmentation becomes noticeably smaller than the width. When the jet inclination angle reaches 60° and 65° , the trend in width variation is the most pronounced, but the depth of fragmentation is the smallest. The volume of fragmented rock shows a significant increase from 0° to 20° , with the maximum volume occurring at 20° . It then decreases from 20° to 40° and increases again from 40° to 60° , but the increase is not as significant as the initial increase from 0° to 20° . From the change trend, it can be found that the corresponding inflection point of the crushing pit formed by the 20° and 40° jets corresponds to the curve, indicating that the impact

crushing effect is gradually enhanced from 0° to 20° and weakens with the increase of the inclination angle.

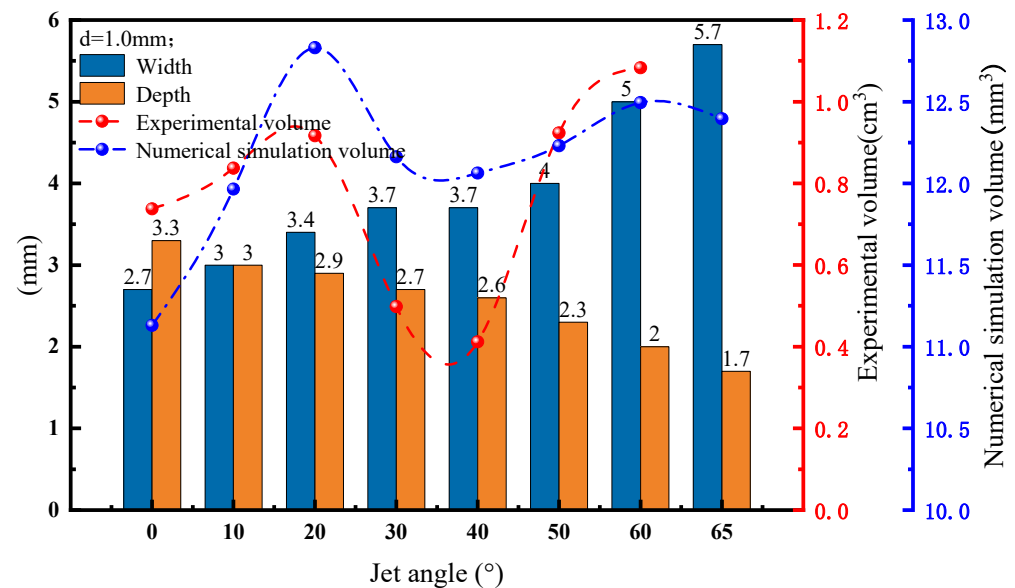


Figure 15. Rocks break the law of jets at different angles.

By analyzing the changes in the flow field of the jet at different inclination angles, it can be concluded that the axial and radial impact forces of the jet vary with the inclination angle. The axial impact force decreases with increasing inclination angle, while the radial impact force increases with increasing inclination angle. Additionally, since the compressive strength of the rock is much higher than its tensile strength, and in the case of inclined impact, rock damage is primarily caused by tensile failure, it can be inferred that as the jet inclination angle increases, the width of fragmentation caused by the jet impact becomes larger while the depth of fragmentation becomes smaller. Therefore, when using a multi-nozzle jet for drilling, it is advisable to employ low inclination angles for rock fragmentation and combine them with high inclination angles for borehole expansion. However, in the numerical simulation, 0° rock breaking volume is the smallest, 20° is the largest, 40° is the smallest, and 20° is the largest in the experiment, indicating that the smaller the inclination angle, although the impact capacity is enhanced, the overall crushing efficiency is lower. The large inclination angle increases the crushing width, resulting in an increase in the volume of broken rock. Through numerical simulation and experimental analysis, the rationality of choosing 20° , 30° , and 60° jet combinations is more clearly determined.

4.3.2. Rotational Rock Breaking Process

In order to further explore the impact rock-breaking characteristics of porous jets, the dynamic pore formation process of multi-nozzle jet impact rock-breaking is analyzed, as shown in Figure 16. Figure 16a–h shows the shape of the hole from the beginning of the hole formation to the complete hole formation of the jet impact rock. From Figure 16a, it can be seen that the jet begins to break the rock and form two crushing pits at 25 μs ; at this time, it is the 20° or 30° jet that begins to break. As the breaking time increases to 50 μs , the 60° jet begins to break the rock, at which time three jets with different inclination angles begin to impact the rock-breaking, and under rotational conditions, different shapes as shown in Figure 16c,d,f are formed at different times, and finally a complete crushing pit is formed at 5000 μs .

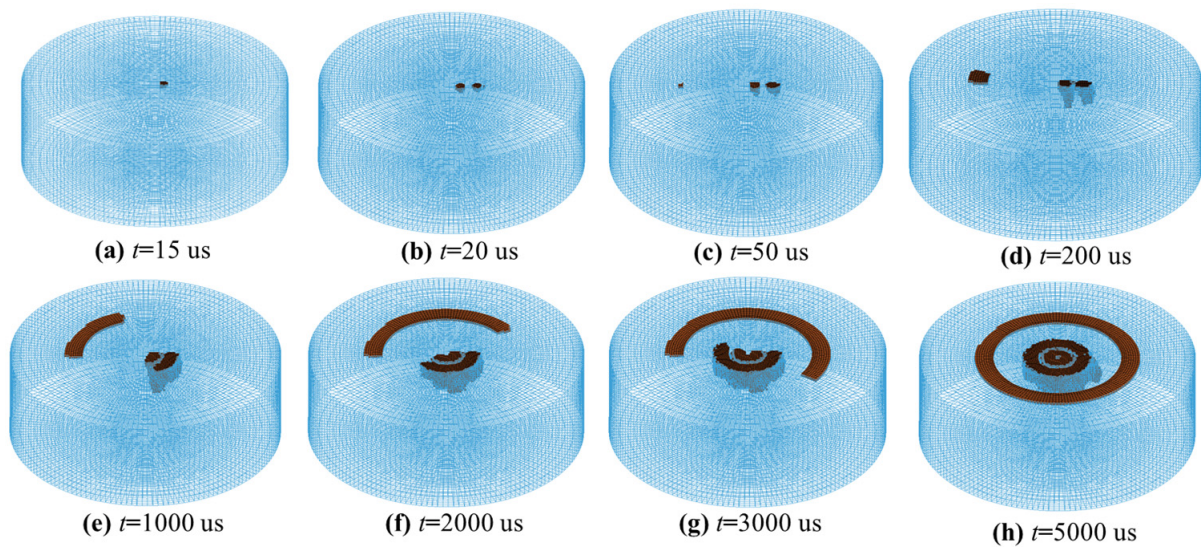


Figure 16. Dynamic hole-forming process.

4.3.3. Analysis of the Forces Acting on Multi-Nozzle Jets

An analysis of the forces acting on rock breaking efficiency is undoubtedly important. However, it is also essential to analyze the forces generated by the jet during the rock-breaking process. By analyzing the stress variation curve during the rock's deformation and failure processes, the characteristics of rock deformation and failure can be better understood. Based on the previous analysis of rock breaking by different inclined jets, we selected the 20° , 30° , and 60° jets for the force analysis of the multi-nozzle jet impact. As shown in Figure 16, it presents three micro-units, H839305, H834905, and H860105, corresponding to the 20° , 30° , and 60° jets directly below, as shown in Figure 17. The mechanical changes that occur in these micro-units under the impact of the jet are analyzed to determine their main failure modes.

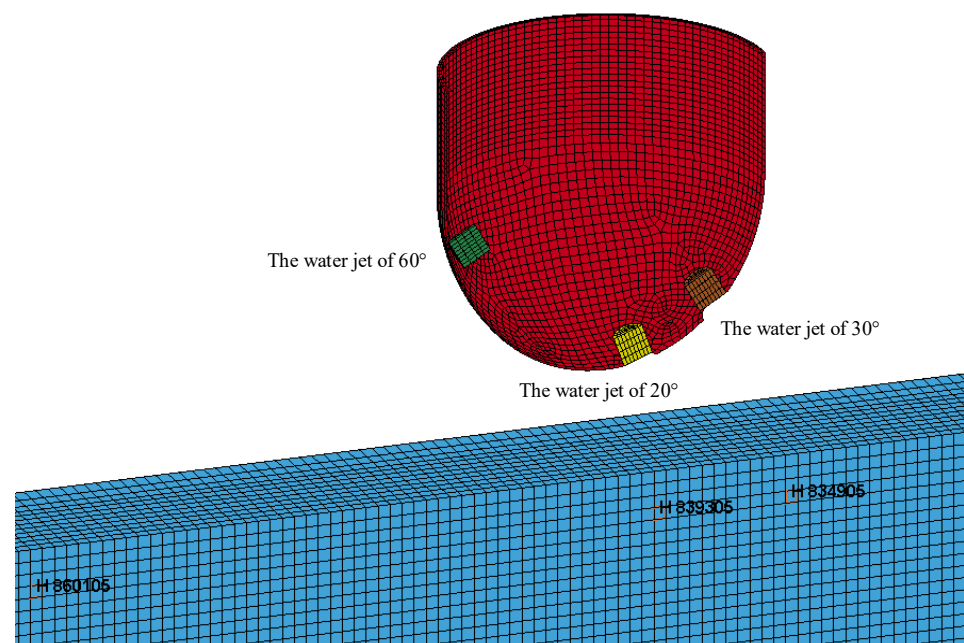


Figure 17. Distribution of selected reference elements.

Figure 18 shows the change curve of the force state of the micro-unit under different inclination angles when the multi-nozzle jet impacts and breaks the rock. This curve clearly reflects that the main failure form of the rock under the impact of a high-pressure water jet is tensile failure caused by unloading. As can be seen from Figure 18a–c, when the jet is in contact with the rock surface, due to the impact of the high-speed jet, a certain compressive stress is generated on the rock surface. From the analysis of the force changes of the three micro-units, it is found that the pressure values of the units H839305 and H834905 are the largest, which are 18.16 MPa and 15.25 MPa, respectively, and the corresponding maximum principal stress values are -13.52 MPa and -9.95 MPa, respectively; the effective stress of the H860105 unit. The maximum value is 8.46 MPa, and the maximum value of the maximum principal stress is 2.7 MPa. It can be seen that the smaller the angle of the jet, the greater the impact pressure on the rock, the stronger the impact, and the greater the the depth of the rock; when the jet inclination is greater, the pressure on the micro-unit decreases, and the rock is under pressure at this time. It is broken under the combined action of stress and shearing force.

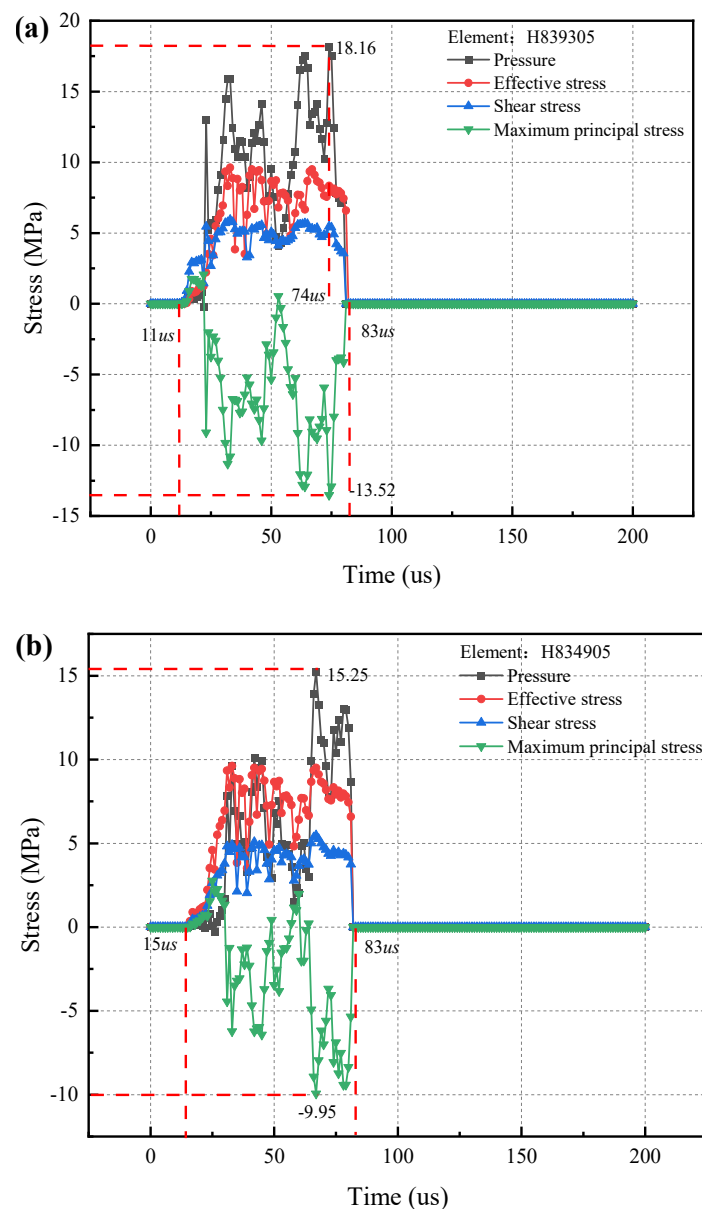


Figure 18. Cont.

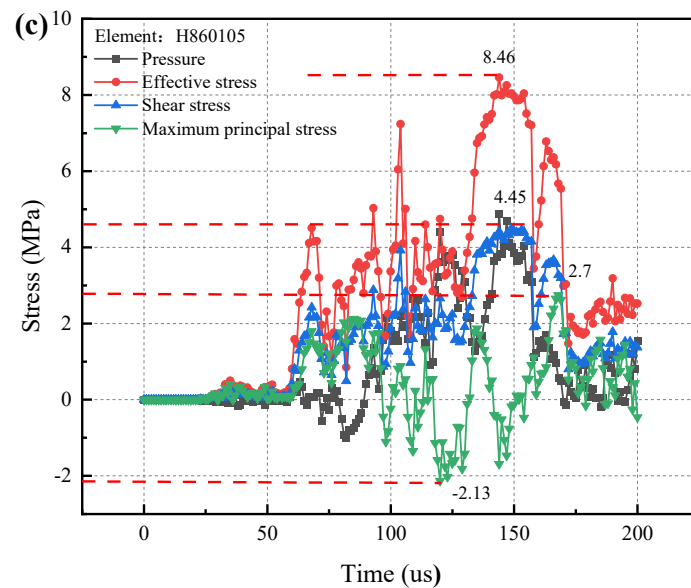


Figure 18. Force variation curve of a rock micro-unit.

The micro-unit H839305 shown in Figure 18a began to be affected by the impact force of the jet at 11 us. With the extension of the jet time, the internal energy of the rock changes rapidly. When the impact time reaches 74 us, the pressure on the jet is the largest. Until 83 us, the micro-unit is completely destroyed, and the effective stress and shear stress are rapidly reduced. The force of unit H834905 shown in Figure 18b is consistent with the force of unit H834905 in Figure 18a, and the maximum pressure and maximum principal stress are both less than the 20° jet. The jet shear force of the unit H860105 by the jet is 4.45 MPa. Through comparison, it can be found that the maximum principal stress values in Figure 18a,b are both greater than the shear stress, while the shear stress value in Figure 18c is greater than the maximum principal stress value, which also indicates that when 20° and 30° jets impact the rock surface, there is a certain impact effect on the rock below the 60° jet farther away, but the impact strength is limited, so this part of the impact can be ignored.

When the jet hits the rock surface, cracks begin to form due to the impact force, and the compressed rock in the jet contact area can release the compression energy laterally. This process causes the rock to exhibit tensile failure. In addition, when the water jet hits the rock's surface, it moves in a radial direction. A jet with a small inclination angle has a larger axial impact force, while when the inclination angle is greater than 45°, the radial impact force is larger. This process also produces a certain stretching effect on the rock. The combined effect of these two states results in the failure of the rock surface from the initial cracks outward in the radial direction.

5. Conclusions

This study conducted rock-breaking experiments using a self-designed test platform. The influence of jet inclination angle, different combinations of multi-nozzles, rotational speed, and target distance on rock-breaking efficiency was analyzed. Additionally, stress analysis of rock subjected to multi-nozzle jet impact was performed using the ALE-FEM coupling method. The main conclusions are as follows:

(1) The jet inclination angle has a significant impact on rock fragmentation efficiency. Through the experiments, it was determined that the optimal combination for multi-nozzle jet drilling involves using a small inclination angle for rock breaking and a large inclination angle for auxiliary hole expansion. The optimal jet combination angles obtained from the experiments were 20°, 30°, and 60°, providing further guidance for multi-nozzle jet experiments;

(2) The effects of target distance and rotational speed on rock breaking efficiency were analyzed using controlled variable experiments. It was found that larger target distances result in larger blind spots in rock fragmentation, while smaller target distances lead to smaller-diameter rock breaking holes. Additionally, the experiments revealed an optimal rotational speed range, which not only affects the number of jet impacts on the rock but also influences the jet divergence capability. The optimal rotational speed range determined in this study was 200 rpm to 400 rpm;

(3) Based on the ALE-FEM coupling method, a novel numerical simulation approach for multi-nozzle jet impact on rock breaking was proposed. The experiments validated that the primary failure modes during rock fragmentation are impact failure induced by compressive stress and shear failure induced by shear stress. The study also clarified the interference effects of stress waves during multi-nozzle jet rock breaking. This method provides new insights for the investigation of the mechanism of multi-nozzle jet rotational rock breaking.

Author Contributions: Conceptualization, Y.L. and L.H.; methodology, L.H.; software, K.S.; validation, Q.B.; formal analysis, L.H.; investigation, L.H.; resources, Y.L.; data curation, L.H.; writing—original draft preparation, L.H.; writing—review and editing, L.H.; visualization, K.S.; supervision, Q.B.; project administration, K.S.; funding acquisition, L.D. All authors have read and agreed to the published version of the manuscript.

Funding: This work is financially supported by the Natural Science Foundation of Chongqing (cstc2021jcyj-msxmX0564, CSTB2022NSCQ-MSX1080), which is gratefully acknowledged.

Institutional Review Board Statement: Not applicable.

Informed Consent Statement: Not applicable.

Data Availability Statement: The data used to support the findings of this study are included within the article.

Acknowledgments: The authors also thank the editor and anonymous reviewers very much for their valuable advice.

Conflicts of Interest: The authors declare no conflict of interest.

References

1. Lu, T.K.; Zhao, Z.J.; Hu, H.F. Improving the gate road development rate and reducing outburst occurrences using the waterjet technique in high gas content outburst-prone soft coal seam. *Int. J. Rock Mech. Min. Sci.* **2011**, *48*, 1271–1282. [[CrossRef](#)]
2. Yang, X.L.; Wen, G.C.; Dai, L.C.; Sun, H.T.; Li, X.L. Ground Subsidence and Surface Cracks Evolution from Shallow-Buried Close-Distance Multi-seam Mining: A Case Study in Bulianta Coal Mine. *Rock Mech. Rock Eng.* **2019**, *52*, 2835–2852. [[CrossRef](#)]
3. Carl, L. Method and Apparatus for Horizontal Well Drilling. U.S. Patent 5,413,184, 9 May 1995.
4. William, G.B. Method and Apparatus for Jet Drilling Drain Holes from Wells. U.S. Patent 6263984B1, 24 July 2001.
5. Lu, Y.Y.; Xiao, S.Q.; Ge, Z.L.; Zhou, Z.; Deng, K. Rock breaking Properties of Multi-Nozzle Bits for Tree-Type Drilling in Underground Coal Mines. *Energies* **2016**, *9*, 249. [[CrossRef](#)]
6. Lu, Y.Y.; Huang, S.; Ge, Z.L.; Zhou, Z.; Liu, W.C.; Guan, Y.R. Research progress and strategic thinking of coal mine waterjet technology to enhance coal permeability in China. *J. China Coal Soc.* **2022**, *47*, 3189–3211.
7. Xu, Y.; Liu, Y.W.; Xu, Y.J.; Zhang, Y.Y. Rock Breaking Characteristics of Ultra-high Pressure Jet with Nozzle Combinations. *Chin. J. Comput. Phys.* **2011**, *28*, 686–692.
8. Chi, H.P.; Li, G.S.; Liao, H.L.; Tian, S.C.; Song, X.Z. Effects of parameters of self-propelled multi-orifice nozzle on drilling capability of water jet drilling technology. *Int. J. Rock Mech. Min. Sci.* **2016**, *86*, 23–28. [[CrossRef](#)]
9. Zhang, T.; Li, Y.M.; Lu, H.; Jiang, J.N. Simulation and Experimental Study on Characteristics of Multiorifice Nozzle in Radial Jet Drilling. *Geofluids* **2022**, *2022*, 1–8. [[CrossRef](#)]
10. Cao, S.R.; Ge, Z.L.; Zhang, D.; Zhou, Z.; Lu, Y.Y.; Zhao, H.Y. An experimental study of ultra-high pressure water jet-induced fracture mechanisms and pore size evolution in reservoir rocks. *Int. J. Rock Mech. Min. Sci.* **2022**, *150*, 104995. [[CrossRef](#)]
11. Lu, Y.Y.; Xiao, S.Q.; Ge, Z.L.; Zhou, Z.; Ling, Y.F.; Wang, L. Experimental study on rock breaking performance of water jets generated by self-rotatory bit and rock failure mechanism. *Powder Technol.* **2019**, *346*, 203–216. [[CrossRef](#)]
12. Liao, H.L.; Niu, J.L.; Cheng, Y.X.; Huang, Z.W.; Ma, D.J. Experiment study on water jet breaking rock by multi-orifice nozzle. *J. China Coal Soc.* **2011**, *36*, 1858–1862.

13. Li, J.B.; Li, G.S.; Huang, Z.W.; Song, X.Z.; Li, K. Flow Field Study on a New Kind Swirling Multi-orifices Nozzle. *Fluid Mach.* **2015**, *43*, 32–41.
14. Reinsch, T.; Paap, B.; Hahn, S.; Wittig, V.; Van den Berg, S. Insights into the radial water jet drilling technology Application in a quarry. *J. Rock Mech. Geotech. Eng.* **2018**, *10*, 236–248. [[CrossRef](#)]
15. Ma, J.J.; Zhao, J.X.; Lin, Y.X.; Liang, J.G.; Chen, J.J.; Chen, W.X.; Huang, L.C. Study on Tamped Spherical Detonation-Induced Dynamic Responses of Rock and PMMA Through Mini-chemical Explosion Tests and a Four-Dimensional Lattice Spring Model. *Rock Mech. Rock Eng.* **2023**. [[CrossRef](#)]
16. Liao, H.L.; Li, G.S.; Niu, J.L.; Chi, H.P.; Huang, Z.W.; Ma, D.J. Rock Breakage Characteristics of Integrating Straight and Swirling Jet Bit for Radial Horizontal Drilling. *J. Basic Sci. Eng.* **2016**, *21*, 471–478.
17. Liao, H.; Wu, D.; Wang, L.; Zhu, L. Comparisons of spraying structure and rock breakage characteristics of round straight, swirling, and straight-swirling integrated jets. *At. Sprays* **2013**, *23*, 363–377. [[CrossRef](#)]
18. Ma, D.J.; Li, G.S.; Zhang, X.N.; Huang, Z.W. Experimental Study on Rock Breaking by A Combined Round Straight Jet with A Swirling Jet Nozzle. *At. Sprays* **2011**, *21*, 645–653. [[CrossRef](#)]
19. Du, P.; Lu, Y.Y.; JR, T.; Zhou, H.; Zhang, W.F. Characteristics and Mechanism of Rock Breaking for New Type Straight-Swirling Integrated Jet. *J. Xi'an Jiaotong Univ.* **2016**, *50*, 81–89.
20. Zhao, G.X.; Fu, T. A Unit Compound Structure Design: Poisson's Ratio Is Autonomously Adjustable from Negative to Positive. *Materials* **2023**, *16*, 1808. [[CrossRef](#)]
21. Si, H.; Wang, D.D.; Li, X.H. Stress wave effect in numerical simulation on rock breaking under high-pressure water jet. *J. Chongqing Univ.* **2008**, *31*, 942–945.
22. Zhao, J.; Zhang, G.C.; Xu, Y.J.; Wang, R.H.; Zhou, W.D.; Han, L.X.; Zhou, Y. Mechanism and effect of jet parameters on particle waterjet rock breaking. *Powder Technol.* **2017**, *313*, 231–244. [[CrossRef](#)]
23. Jiang, H.X.; Liu, Z.H.; Gao, K.D. Numerical simulation on rock fragmentation by discontinuous water-jet using coupled SPH/FEA method. *Powder Technol.* **2017**, *312*, 248–259. [[CrossRef](#)]
24. Liu, X.H.; Liu, S.Y.; Ji, H.F. Numerical research on rock breaking performance of water jet based on SPH. *Powder Technol.* **2015**, *286*, 181–192. [[CrossRef](#)]
25. Xue, Y.Z.; Si, H.; Chen, G.H. The fragmentation mechanism of coal impacted by water jets and abrasive jets. *Powder Technol.* **2020**, *361*, 849–859. [[CrossRef](#)]
26. Xue, Y.Z.; Si, H.; Xu, D.Y.; Yang, Z.L. Experiments on the microscopic damage of coal induced by pure water jets and abrasive water jets. *Powder Technol.* **2018**, *332*, 139–149. [[CrossRef](#)]
27. Ni, H.J.; Wang, R.H.; Zhang, Y.Q. A Study of the Rock Breaking Mechanism during Swirling Water Jet Drilling. *Appl. Math. Mech.* **2005**, *26*, 1445–1452.
28. Ma, J.J.; Chen, J.J.; Guan, J.W.; Lin, Y.X.; Chen, W.X.; Huang, L.C. Implementation of Johnson-Holmquist-Beissel model in four-dimensional lattice spring model and its application in projectile penetration. *Int. J. Impact Eng.* **2023**, *170*, 104340. [[CrossRef](#)]
29. Yang, X.; He, L.; Lu, T.; Liu, Y.; Li, X.; Cao, J.; Luo, G.; Yang, H. Optimization and field application of water jet for coal bed methane stimulation. *Energy Sci. Eng.* **2019**, *7*, 3186–3203. [[CrossRef](#)]
30. Liu, Y.B.; Ba, Q.B.; He, L.P.; Shen, K.; Xiong, W. Study on the rock-breaking effect of water jets generated by self-rotatory multi-nozzle drilling bit. *Energy Sci. Eng.* **2020**, *8*, 2457–2470. [[CrossRef](#)]
31. He, L.P.; Liu, Y.B.; Shen, K.; Yang, X.L.; Quan, Q.B.; Xiong, W. Numerical research on the dynamic rock-breaking process of impact drilling with multi-nozzle water jets. *J. Pet. Sci. Eng.* **2021**, *207*, 109145. [[CrossRef](#)]
32. Lu, Y.Y.; Huang, F.; Liu, X.X.; Ao, X. On the failure pattern of sandstone impacted by high-velocity water jet. *Int. J. Impact Eng.* **2015**, *76*, 67–74. [[CrossRef](#)]
33. Holmquist, T.J.; Johnson, G.R.; Cook, W.H. A computational constitutive model for concrete subjected to large strains, high strain rates and high pressures. In Proceedings of the 14th International Symposium on Ballistics, Quebec, QC, Canada, 26–29 September 1993; pp. 591–600.

Disclaimer/Publisher's Note: The statements, opinions and data contained in all publications are solely those of the individual author(s) and contributor(s) and not of MDPI and/or the editor(s). MDPI and/or the editor(s) disclaim responsibility for any injury to people or property resulting from any ideas, methods, instructions or products referred to in the content.